International Journal of Nanomedicine

Dovepress
open access to scientific and medical research

Open Access Full Text Article

ORIGINAL RESEARCH

Improved Immunoregulation of Ultra-Low-Dose Silver Nanoparticle-Loaded TiO_2 Nanotubes via M2 Macrophage Polarization by Regulating GLUT1 and Autophagy

This article was published in the following Dove Press journal:
International Journal of Nanomedicine

Yangmengfan Chen,[1,*] Ming Guan,[1,*] Ranyue Ren,[1] Chenghao Gao,[1] Hao Cheng,[2] Yong Li,[1] Biao Gao,[3] Yong Wei,[3] Jijiang Fu,[3] Jun Sun,[4] Wei Xiong[1]

[1]Department of Orthopedics, Tongji Hospital, Tongji Medical College, Huazhong University of Science and Technology, Wuhan 430030, People's Republic of China; [2]Department of Orthopedics, Nanfang Hospital, Southern Medical University, Guangzhou 510515, People's Republic of China; [3]The State Key Laboratory of Refractories and Metallurgy, School of Materials and Metallurgy, Wuhan University of Science and Technology, Wuhan 430081, People's Republic of China; [4]Department of Biochemistry and Molecular Biology, Basic Medical School, Tongji Medical College, Huazhong University of Science and Technology, Wuhan 430030, People's Republic of China

*These authors contributed equally to this work

Correspondence: Jun Sun
Department of Biochemistry and Molecular Biology, Basic Medical School, Tongji Medical College, Huazhong University of Science and Technology, Wuhan 430030, People's Republic of China
Tel +86 189 7128 0215
Email sunjun99@hotmail.com

Wei Xiong
Department of Orthopedics, Tongji Hospital, Tongji Medical College, Huazhong University of Science and Technology, 1095 Jiefang Avenue, Wuhan 430030, People's Republic of China
Tel +86 132 1273 6006
Email 1996tj0558@hust.edu.cn

Introduction: The bone regeneration of endosseous implanted biomaterials is often impaired by the host immune response, especially macrophage-related inflammation which plays an important role in the bone healing process. Thus, it is a promising strategy to design an osteo-immunomodulatory biomaterial to take advantage of the macrophage-related immune response and improve the osseointegration performance of the implant.

Methods: In this study, we developed an antibacterial silver nanoparticle-loaded TiO_2 nanotubes (Ag@TiO_2-NTs) using an electrochemical anodization method to make the surface modification and investigated the influences of Ag@TiO_2-NTs on the macrophage polarization, osteo-immune microenvironment as well as its potential molecular mechanisms in vitro and in vivo.

Results: The results showed that Ag@TiO_2-NTs with controlled releasing of ultra-low-dose Ag^+ ions had the excellent ability to induce the macrophage polarization towards the M2 phenotype and create a suitable osteo-immune microenvironment in vitro, via inhibiting PI3K/Akt, suppressing the downstream effector GLUT1, and activating autophagy. Moreover, Ag@TiO_2-NTs surface could improve bone formation, suppress inflammation, and promote osteo-immune microenvironment compared to the TiO_2-NTs and polished Ti surfaces in vivo. These findings suggested that Ag@TiO_2-NTs with controlled releasing of ultra-low-dose Ag^+ ions could not only inhibit the inflammation process but also promote the bone healing by inducing healing-associated M2 polarization.

Discussion: Using this surface modification strategy to modulate the macrophage-related immune response, rather than prevent the host response, maybe a promising strategy for implant surgeries in the future.

Keywords: silver nanoparticle, TiO_2 nanotubes, immune response, glucose transport, autophagy

Introduction

Owing to the outstanding mechanical property, chemical stability and biocompatibility, titanium (Ti) alloy implants have been widely used for orthopedic and dentistry surgeries to restore damaged tissue and structure during the past decades.[1] However, many undesirable complications occurred after surgery, especially poor osteointegration and bacterial infection.[2] To further avoid adverse events and optimize the performance of implants, nano-surface modification may be a promising strategy and become one of the recent research hotspots. For example,

titanium dioxide nanotubes (TiO_2-NTs) have been proven to be effective in promoting osteogenesis,[3] regulating immune response,[4] and killing bacteria.[5] Besides, TiO_2-NTs are considered as a new kind of surface strategy for controlled drug delivery systems, such as silver nanoparticles (AgNPs) which can prevent infection with the broad-spectrum antimicrobial property.[6] However, a considerable level of cytotoxicity will be invoked by the inappropriate therapeutic window concentration of Ag^+ ions, which greatly limits the clinical application.[7]

In our previous studies, Cheng et al showed that the AgNPs loaded TiO_2-NTs (Ag@TiO_2-NTs) with low dose Ag^+ releasing exhibited simultaneous antimicrobial and excellent bio-integration properties.[8,9] Besides, Ag@TiO_2-NTs with a lower initial concentration (0.14ppm) of Ag^+ ions also achieved an excellent synergistic antibacterial capacity in combination with antibiotics both in vitro and in vivo.[10] Interestingly, it has recently been reported that the AgNPs-loaded biomaterials with continuing releasing extremely low dose Ag^+ could enhance cell adhesion,[10] spreading,[11] proliferation,[12] reactive oxygen species (ROS) scavenging,[11] and new bone formation[13] by the unique controlled-release characteristic and topographic feature.

Despite the number of studies that have been conducted, only a few biomaterials are successfully used in clinical practice because of the complex network of immune microenvironment.[14] Some implants may induce abundant new bone formation in vitro, while losing the osteointegration efficiency and even elicit the formation of a surrounding inflammatory fibrous in vivo.[14] This phenomenon has been proven to be related to the host immune response. The early host immune response leads to a specific "immune niche", which recruits immune cells and secretes various cytokines.[15] Besides, macrophage plays a representative role in the early host immune response that initially recognizes the foreign bodies and promotes to create the pro-inflammatory or pro-wound healing microenvironment.[16] Similar to Th1/Th2 cells, macrophages can be polarized into two major phenotypes, namely, pro-inflammatory M1 phenotype and wound-healing M2 phenotype.[17] M1 macrophages are induced by interferon-γ or lipopolysaccharide, and secrete pro-inflammatory cytokines including interleukin-1β (IL-1β), inducible nitric oxide synthase (iNOS), tumor necrosis factor α (TNF-α) and reactive oxygen species (ROS), to promote inflammation and impair implants. In contrast, M2 macrophages are induced by cytokines IL-4 and IL-10,[18,19] and secrete anti-inflammatory cytokines such as IL-10, along with various growth factors such as transforming growth factor β (TGF-β), vascular endothelial growth factor (VEGF), 1,25-dihydroxy vitamin D3 and bone morphogenetic protein (BMP) to suppress inflammation, promote extracellular matrix reconstruction and bone healing.[20–22] Recent studies have shown that the presence of chronic M1 macrophage at the bone–implant interface inhibited new bone formation and promoted implant inflammatory encapsulation.[26] In addition, a greater ratio of M1/M2 macrophage has been found a high correlation with the failure of artificial joints surgeries.[23] Therefore, regulating the proportion of M1/M2 macrophage and promoting macrophage polarization towards M2 phenotype may be critical to suppress local undesired inflammation, obtain a proper immune response and promote tissue regeneration.[24]

Many studies have revealed that biomaterials designed for controlling cellular activities could regulate glucose metabolism by harnessing the expression of glucose transporters or glycolytic enzymes.[25,26] Besides, ATP produced by glucose metabolism can meet energy demands for many cellular activities, such as enzyme reaction, and electron transfer.[27] However, cellular metabolism not only provides the source of energy but also involves the inflammatory response.[28] For example, the glucose transporter 1 (GLUT1) which plays a key role in glucose uptake and glycolysis, can regulate the secretion of pro-inflammatory cytokines within macrophages.[29] Our previous study has proven that Ag@TiO_2-NTs could enhance cell adhesion, spreading, and ROS-scavenging,[11] but it is unclear about the specific role of glucose metabolism playing in these cellular processes. To further explore the influence of Ag@TiO_2-NTs on the osteo-immune microenvironment, we attempted to study the effects of glucose metabolism in macrophages.

Highly correlated with energy metabolism,[30] autophagy is a kind of highly conserved and ubiquitous cellular activity for maintaining homeostasis via the degradation of redundant and impaired intracellular components.[31] Autophagy may also regulate the cellular differentiation under the various conditions, such as oxygen, cytokines, as well as the innate and adaptive immune systems.[30,32] For example, the impaired skin, muscle and bone during the implant surgery will generate oxidative stress around the interface of tissue-implant.[2] As a result, inflammation mediators and ROS will be produced at local and promoted macrophages to polarize into M1 phenotype with a pro-inflammatory microenvironment. However, autophagy has been found to have an anti-inflammatory effect to promote M2 macrophage differentiation via inhibition

of inflammasomes and ROS.[33–37] Therefore, stimulating autophagy to regulate osteo-immune microenvironment via scavenging ROS is feasible.

The phosphoinositide 3-kinase (PI3K)/protein kinase B (Akt) signaling pathway is an important intracellular signaling pathway, which plays an essential role in cell growth, metabolism and polarization.[4,38] It has been proven that many factors are capable to affect GLUTs by regulating the PI3K/Akt signaling pathway, and control the glucose uptake.[39] In addition, as a downstream target of the PI3K/Akt pathway, mTOR facilitates anabolic metabolism and inhibits autophagy induction.[40]

In the present study, we fabricated the Ag@TiO_2-NTs with controlled releasing of ultra-low-dose Ag^+ ions using an electrochemical anodization method and investigated the immune-regulatory influences of Ag@TiO_2-NTs on the macrophage polarization, osteo-immune microenvironment as well as its molecular mechanisms in vitro and in vivo. The results showed that Ag@TiO_2-NTs could not only inhibit the inflammation process but also promote the bone healing by inducing healing-associated M2 polarization. This strategy may be promising for clinical applications and provide new insights into the surface modification of biomaterials.

Materials and Methods

Specimen Preparation

Ti plate (purity: 99.7%,10×10×1 mm^3, Aldrich) and Ti rods (the diameter is 0.8 mm; the length is 12 mm) were purchased from Sigma-Aldrich and polished by SiC sandpapers, followed by degreasing sequentially with acetone, ethanol, and distilled water, and then dried by nitrogen gas. The preparation method of electrochemical anodization was detailed described in our previous work.[9] Briefly, electrodes were placed 1 cm apart and soaked in electrolyte of ethylene glycol consisting of ammonium fluoride (NH_4F, 0.5%) and distilled deionized water (5%). Ti specimens were used as the anode electrode, and graphite foils were used as the cathode electrode. The amorphous TiO_2-NTs were constructed on the Ti specimens after anodization under direct current (DC) at 60 V for 1 h. Then, the amorphous form would convert to anatase to strengthen the bonds between the Ti matrix and the NTs after annealing at 450°C for 3 h in a tube furnace. To prepare Ag@TiO_2-NTs, we soaked the anatase TiO_2-NTs in the $AgNO_3$ solution (1 M, purity>99.8%) for 10 mins. After that, the specimens were rinsed gently with distilled deionized water, dried in air and exposed to ultraviolet (UV) irradiation of a high-pressure Hg lamp for 30 mins to strengthen the bonding of the Ag to the inner surface of the NTs. Besides, the silver nanoparticles suspension (20nm, Sigma-Aldrich, USA) were used for the supplementary test.

Nanostructure, Surface Characterization, and Ag^+ Release

The surface topography of specimens (Ti, TiO_2-NT, and Ag@TiO_2-NT) were evaluated by scanning electron microscopy (SEM; FEI Nova400 Nano, USA) and transmission electron microscopy (TEM; Philips CM20, Amsterdam, The Netherlands). The chemical composition of the specimens was detected by X-ray photoelectron spectroscopy (XPS; ESCALAB MK-II, VG, USA) and energy-dispersive X-ray spectrometry (EDS; Tecnai). We used the Total Antioxidant Capacity Assay Kit (Beyotime, China) and the ferric reducing ability of plasma (FRAP) method to evaluate the antioxidant capacity of different specimens. In brief, all samples were immersed in 500 μL the FRAP solution and incubated at 37°C for 5 min. Then we transferred the solution to the 96-well plate and measured the fluorescence intensity at the 590nm by using the spectrophotometer (Bio Tek Instruments Inc., USA). The Ag^+ ions release from the Ag@TiO_2-NTs was measured as follows. First, each Ag@TiO_2-NT was immersed in 4 mL phosphate-buffered saline (PBS) in dark at room temperature, with PBS refreshing every 24h. To test the Ag^+ ions release quantity, the collected PBS was analyzed by inductively coupled plasma–atomic emission spectrometry (ICP-AES; Thermos Elemental IRIS Advantage, USA) at day 1, 3, 5, 7, and 10, with the specific emission line of 328.1 nm for Ag.

Cell Culture

The RAW 264.7 macrophages and MC3T3-E1 pre-osteoblasts (The Shanghai Cell Bank of the Chinese Academy of Sciences, China) were used in this study. RAW 264.7 cells were cultured in DMEM (Gibco, USA) that contains 10% fetal bovine serum (Gibco, USA) and 1% penicillin/streptomycin in a humidified atmosphere containing 5% CO_2 at 37°C. The culture medium was changed every day. The cells were passaged by dislodging from the flask surface using a cell scraper. An inhibitor of autophagy (3-MA; 1 mM, Selleck, USA), activator of autophagy (rapamycin; 100 nM, Selleck, USA), the inhibitor of GLUT1 (STF31; 10uM, Selleck, USA) and PI3K

activator (740Y-P; 10 uM, Selleck, USA) were used. MC3T3-E1 pre-osteoblasts were maintained in α-MEM (Gibco, USA) containing 10% fetal bovine serum and 1% penicillin–streptomycin in a humidified atmosphere containing 5% CO_2 at 37°C. The culture medium were changed every 3 days, and the cells were passaged upon reaching 80% confluence by dislodging from the flask surface using trypsin.

Cell Proliferation and Morphology

RAW 264.7 macrophages were cultured on Ti, TiO_2-NTs, and Ag@TiO_2-NTs (1×1 cm^2). The cell proliferation was evaluated by using the CCK-8 kit (Cell Counting Kit-8; Beyotime, China). The cells were cultured for 24h, 48h, and 72h, and then the culture medium was replaced with a 500 μL CCK-8 solution. After 1h of incubation at 37°C, the CCK-8 solution was removed to a 96-well plate, and a quantitatively assayed was carried out by a microplate spectrophotometer (Nikon, Japan) at an absorbance of 450 nm. RAW 264.7 cells (5000 per well) were cultured on the surface of different samples in a 24-well plate and incubated for 24 h at 37°C. After 24h, the unattached cells were removed by rinsing with PBS, then the adherent cells were immersed in paraformaldehyde (PFA, 4%) solution for 10 min, and then stained with phalloidin (5 μg/mL, Sigma, USA) for 30 mins, then 4′,6-diamidino-2-phenylindole (DAPI) for 15 mins in dark. The fluorescence images were obtained by a fluorescence microscope (Nikon, Japan). For SEM images, RAW 264.7 cells were seeded at 5000 per well. After cultured for 24h, the cells growing on the samples were washed with PBS and fixed with 2.5% glutaraldehyde. Then these specimens were dehydrated in a graded ethanol series, and freeze-dried, then coated with gold, and evaluated by the SEM (FEI Nova400 Nano, USA).

M1/M2 Macrophage Polarization

RAW 264.7 cells were cultured on the surfaces of different specimens (2 × 2 cm^2) at 2×10^5 per specimens. Total RNA was extracted from the treated RAW 264.7 cells by using TRIzol reagent (Life Technologies, USA). The cDNA was synthesized from 500 ng total RNA using the SensiFAST™ cDNA Synthesis Kit following the manufacturer's instructions (Toyobo, Japan). The primers used for reverse transcription-quantitative PCR in this study were shown in Table 1. The mRNA expression levels of the target genes (the macrophage markers iNOS and Arginase1) were determined using SYBR Green qPCR Master Mix (Toyobo) on the QuantStudio ™ Real-Time PCR instrument (Toyobo, Japan). The relative expression levels were evaluated by normalizing the cycle threshold (Ct) value of each target gene against that of GAPDH. The ΔΔCt method was used to calculate the fold changes in mRNA expression levels of the TiO_2-NTs and Ag@TiO_2-NTs groups relative to the Ti control group. Proteins related to macrophage phenotype were evaluated by Western blot through using primary antibodies targeting Arginase1, iNOS (1:1000, rabbit anti-mouse; Abcam, UK) and GAPDH (1:5000, rabbit anti-mouse; Abcam, UK). A goat anti-rabbit antibody (Boster, China) at a 1:5000 dilution was used as the secondary antibody. All Western blot bands were quantitated and analyzed (Gel-Pro Analyzer software, USA) based on at least three samples.

ROS Production

Generation of intracellular ROS was evaluated by the ROS-sensitive fluorescent probe 2′,7′-dichlorodihydrofluorescein diacetate (DCFH-DA; Abcam, UK). The RAW 264.7 cells on Ti, TiO_2-NTs, and Ag@TiO_2-NTs were cultured for 24h, then incubated with 10 mM DCFH-DA at 37°C for 30 min,

Table 1 Primers Used for Real-Time PCR

Gene	Forward Primer Sequence (5′-3′)	Reverse Primer Sequence (5′-3′)
iNOS	AATCTTGGAGCGAGTTGTGG	CAGGAAGTAGGTGAGGGCTTG
Arginase I	CTCCAAGCCAAAGTCCTTAGAG	AGGAGCTGTCATTAGGGACATC
Beclin I	GGCCAATAGATGGGTCTGA	GCTGCACACAGTCCAGAAA
p62	GACACCCACTACCCCAGAAA	ATCTGTTCCTCTGGCTGTCC
LC3	CACACCCATCGCTGACATCT	GCAGGCCTGAGCAGTCTTTA
ALP	ACATTGCTACACAACTCATCTCC	TCCTGCCATCCAATCTGGTTC
Runx2	GACTGTGGTTACCGTCATGGC	ACTTGGTTTTTCATAACAGCGGA
OCN	CCCAGGCGCTACCTGTATCAA	GGTCAGCCAACTCGTCACAGTC
OPG	CCTTGCCCTGACCACTCTTAT	CACACACTCGGTTGTGGGT
GLUT I	GCAGTTCGGCTATAACACTGG	GCGGTGGTTCCATGTTTGATTG
GAPDH	AGGTCGGTGTGAACGGATTTG	GGGGTCGTTGATGGCAACA

and washed in PBS. ROS production was observed by confocal microscopy (TCS SP5, Leica Microsystem, Germany).

Expression of Autophagy, GLUT1 and p-Akt/Akt in RAW 264.7 Macrophages

The mRNA and protein expression levels of LC3, Beclin1, p62, and GLUT1 were evaluated by qPCR and Western blotting. The primer sequences used for qPCR were listed in Table 1. Primary antibodies targeting LC3, Beclin1, p62, GLUT1 (1:1000, rabbit anti-mouse; Abcam, UK), Akt (1:1000, rabbit anti-mouse; CST, USA), p-Akt (1:1000, rabbit anti-mouse; CST, USA) and GAPDH (1:5000, rabbit anti-mouse; Abcam, UK) were used for Western blotting. A goat anti-rabbit antibody (Boster, China) at a 1:5000 dilution was used as the secondary antibody.

The Co-Cultured Test of Macrophage and Pre-Osteoblasts

The conditioned medium (CM) was collected from the RAW 264.7 cells cultured on various implant groups (Ti, TiO_2-NTs, and Ag@TiO_2-NTs) for 24h. Then the MC3T3-E1 pre-osteoblasts were cultured with the CM for 72h, and the effect of CM on pre-osteoblast differentiation was investigated. The expression of alkaline phosphatase (ALP) and Runt-related transcription factor 2 (RUNX2) was measured by qPCR (primer sequences are shown in Table 1). After culturing for 7 days, pre-osteoblasts were washed with PBS and fixed by paraformaldehyde. Then the staining for ALP was performed using the BCIP/NBT alkaline phosphatase color development kit (Beyotime, China) for 15 min. The stained cells were washed with PBS three times, and images were acquired by a microscope. 21 days after co-culture, the pre-osteoblasts were stained by alizarin red (40 mM, pH 4.2) at room temperature for 10 min and images were acquired by a microscope.

In vivo Animal Experiments

All surgeries in the animal experiments were conducted using protocols approved by the Ethics Committee for Animal Experiments of Huazhong University of Science and Technology, Wuhan, China. All rats in our experiment were treated according to the Guide for the Care and Use of Laboratory Animals (8th edition). This study used a total of 30 adult male Sprague-Dawley rats (SD rats; average weight 150 g), that were obtained from the Laboratory Animal Center of Tongji Medical College, Huazhong University of Science and Technology. All rats were divided into three equal groups, and then implanted with Ti, TiO_2-NTs or Ag@TiO_2-NTs rods for histomorphometry and imaging analysis: group 1 (Ti-rod), group 2 (TiO_2-NTs rod) and group 3 (Ag@TiO_2-NTs rod). The TiO_2-NTs rod and Ag@TiO_2-NTs rod (the diameter is 0.8 mm; the length is 12 mm) for the animal experiments were also fabricated by the method of electrochemical anodization as the same with the Titanium plate above. Details of the surgical procedure were described previously.[9] Briefly, all rats were anesthetized by inhalation of isoflurane before the surgery. The surgical site was disinfected by povidone-iodine after shaving and sterilizing. A surgical incision was made across the right knee and a defect area of 2 mm in diameter using a miniature drill was created in the right tibia of each rat 10 mm below the epiphyseal plate. The volume of bone defect is approximately the same in each rat. Then we used a syringe needle (external diameter is 0.8 mm) to drill a hole at the tibial plateau. The rod of Ti, TiO_2-NTs, and Ag@TiO_2-NTs were implanted into the medullary cavity. After that, the hole was sealed by bone wax. Finally, the skin openings were sutured by clips and sterilized by povidone-iodine.

Micro-Computed Tomography (CT) and X-Ray Evaluation

2 weeks after surgery, X-ray (Kodak, Directview, DR3000) evaluation was performed to monitor the healing status of bone defects and new bone formation. After anesthesia, the tibias with implants were subjected to micro-CT (vivaCT40, Scanco Medical, Switzerland). The micro-CT was performed at 70 kV, 114 μA, the integration time was 300 ms, the resolution was 20 μm. The interested volume was designed with a total of 50 slices 5 mm under the growth plate.[8] The bone volume/tissue volume (BV/TV) ratio was analyzed by the built-in software of our micro-CT instrument.

Histological Analysis and Immunohistochemistry

Each rat was euthanized by overdose CO_2. The right tibia was separated from the surround soft tissue. Then the samples were fixed in 4% paraformaldehyde for 24h. And the right tibias were incubated in ethylenediaminetetraacetic acid, then embedded in paraffin. Specimens were cut into sagittal sections for 5 μm thick. The expression of proteins was assessed using antibodies targeting TNF-α, TGF-β, CD68, LC3, GLUT1 (Abcam, UK), p-Akt (CST, USA) followed by 50 μL polymerized HRP-conjugated anti-mouse/rabbit IgG

(ElivisionTM plus Polymer HRP [mouse/rabbit] IHC Kit). After that, the specimens were stained by Mayer's hematoxylin and then imaged by a light microscope (Nikon E600, Japan).

Statistical Analysis

In this study, all experiments were repeated three times respectively, the results were expressed as means ± standard deviation. One-way analysis of variance (ANOVA) with the Student–Newman–Keuls post hoc test was used to determine statistical significance. Statistically significant differences compared with the control group were considered at $P < 0.05$ (*$P < 0.05$, **$P < 0.01$, ***$P < 0.001$ and ****$P < 0.0001$).

Results and Discussion

Surface Characterization and Ag^+ Release

The surface characteristics of implants are critical for the polarization of macrophages,[41] such as the surface topography, chemistry composition, and hydrophilicity.[42] Figure 1A displayed the SEM images of specimens obtained by electrochemical anodization at 60 V for 1h. Similar to our previous articles,[9,10] a nanoscale tubular surface of TiO_2-NTs was orderly arranged on the Ti substrate and the inner diameter of the TiO_2-NTs was 130–140 nm (Figure 1A). Amancherla Rajyalakshmi et al reported that the number of macrophages adhered on the TiO_2-NTs would decrease with the increasing of tubular diameter, compared with the diameter of 40–50 and 60–70 nm.[43] Meanwhile, the decreased number of $CD68^+$ macrophages had been proved to be a benefit for the osteo-immune microenvironment, which indicated the rationality of our design.[16] Besides, the chemistry composition could also influence cellular activities. TiO_2-NTs incorporated with selenium nanoparticles (SeNPs) could suppress macrophages proliferation,[44] whereas Cu-TiO_2-NTs could promote.[45] In this study, the Ag^+ was reduced by the high-pressure UV-irradiation to fabricate the AgNPs. During this

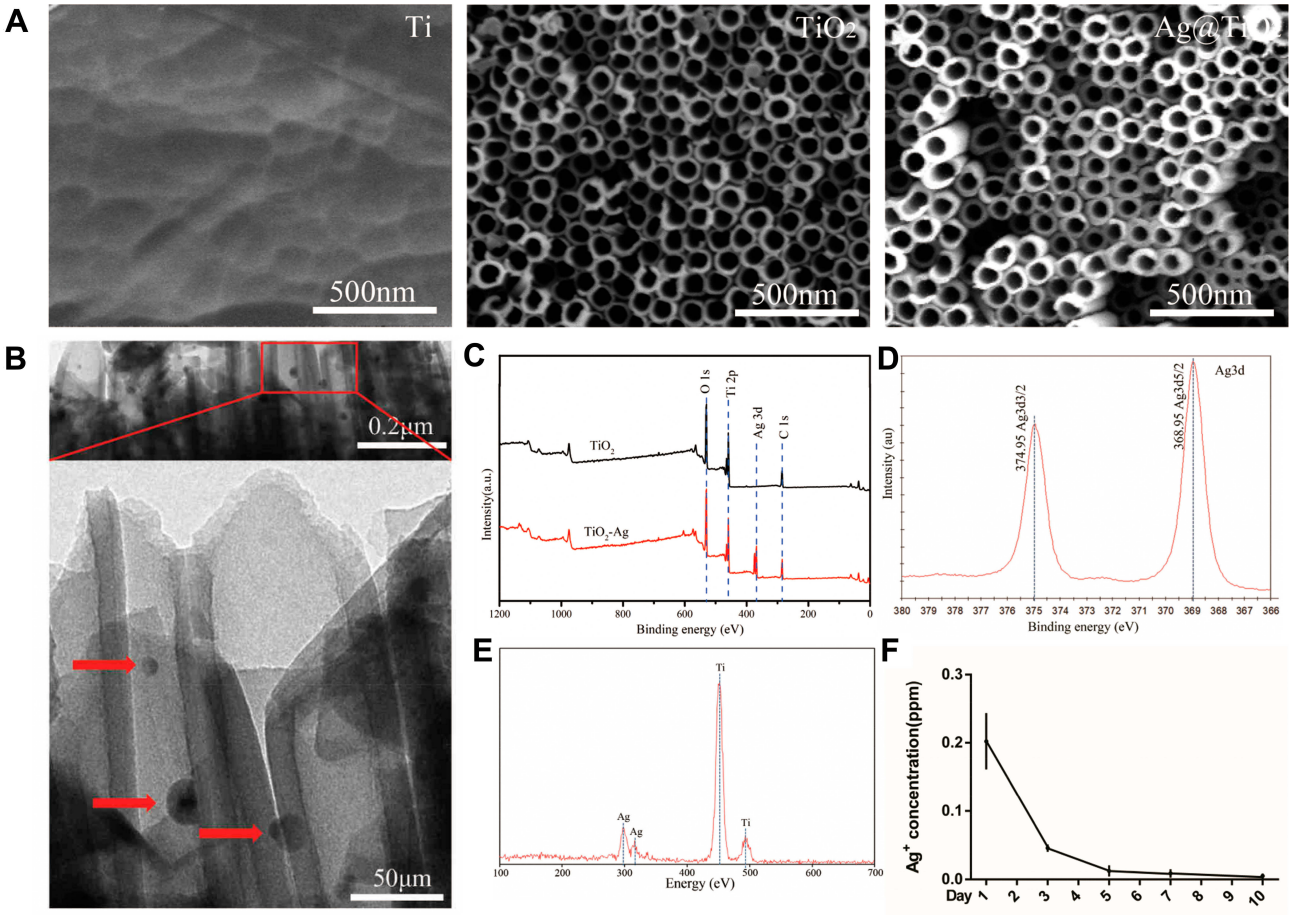

Figure 1 Surface characterization and Ag^+ release. (**A**) the SEM images of nanostructured surfaces of Ti, TiO_2-NTs and Ag@TiO_2-NTs, respectively. (**B**) the images of TEM of Ag@TiO_2-NT (red arrows indicate AgNPs). (**C**) the full XPS spectrum of TiO_2-NTs and Ag@TiO_2-NTs. (**D**) the fine XPS spectrum of Ag3d. (**E**) the EDS spectrum of Ag@TiO_2-NT. (**F**) the curve of Ag ion released from Ag@TiO2-NTs on day 1, 3, 5, 7 and 10. The error bars indicate means ± standard deviations.

method, neither the reducing agent nor heat treatment is needed. The full XPS survey spectrum (Figure 1C) of TiO_2-NTs and Ag@TiO_2-NTs illustrated the chemical components of the specimen surface and the signals of Ag, Ti, C, and O were detected. The C signal was supposed to arise from accidental contamination. Figure 1D showed the fine XPS spectrum of Ag3d and the peaks of Ag3d5/2 and Ag3d3/2 were detected at 368.95 and 374.95 eV, respectively. Meanwhile, Ti and Ag were clearly shown in the EDS curve (Figure 1E). Thus, the results suggested that the AgNPs were successfully loaded on the layer of the TiO_2-NTs. Besides, Figure 1F showed the release kinetics of Ag^+ ions from Ag@TiO_2-NTs detected by ICP-AES on days 1, 3, 5, 7 and 10 was 0.202, 0.046, 0.012, 0.009, and 0.005 ppm, respectively, which decreased gradually after the first 3 days. As with the initial concentration and release kinetics of Ag^+ ions in our previous study,[10] our Ag@TiO_2-NTs could have the excellent antibacterial effect when combined with antibiotics. Meanwhile, the size of AgNPs is an important factor that influences the cytotoxicity. Venugopal et al reported that 10~30 nm AgNPs had no statistical cytotoxicity.[46] In this study, we fabricated the AgNPs from Ag+ by the method of photocatalytic reduction, and the size of AgNPs coated on the TiO_2-NTs layer was satisfied with around 20nm detected by TEM images (Figure 1B).[9,11] For this method, the concentration of the silver salt plays a very important role for both the size and the shape of AgNPs which can be regulated by changing the concentration of $AgNO_3$ solution.[10,47] Therefore, the size of AgNPs always be around 20 nm for the reason that the concentration of the $AgNO_3$ solution was 1M.

Cell Morphology and Proliferation

Cells intend to bind at sharp edges of TiO_2-NTs walls,[48] and the changed cellular morphology usually indicates the direction of cell differentiation.[49] The SEM images (Figure 2A) and phalloidin/DAPI staining (Figure 2B) showed that macrophages that adhered to various surfaces exhibited different morphology. Macrophages cultured on the surface of Ti and TiO_2-NTs formed a more rounded shape, which indicated the differentiation of the M1 phenotype. However, the cells exhibited a more elongated shape on the surface of Ag@TiO_2-NTs, which indicated the differentiation of the M2 phenotype. This results indicated that Ag@TiO_2-NTs played an important role in regulating the functions of macrophages by modulating their cellular morphology which was consistent with other former studies.[16]

For implant biomaterials, the potential cytotoxicity is one of the most concerned problems.[50] The cytotoxicity of AgNPs has been proven to be time- and dose-dependent.[51] However, a suitable low concentration of AgNPs can significantly promote cell proliferation and activity.[52] Both Yunzhu Qian et al and Xuemin Zeng et al reported that the silver-modified implants, of which the total concentration of Ag^+ was below 0.06ppm and 0.12ppm, had the ability to promote cells proliferation and osteogenesis.[12,52] To eliminate the toxic effects of AgNPs on cellular

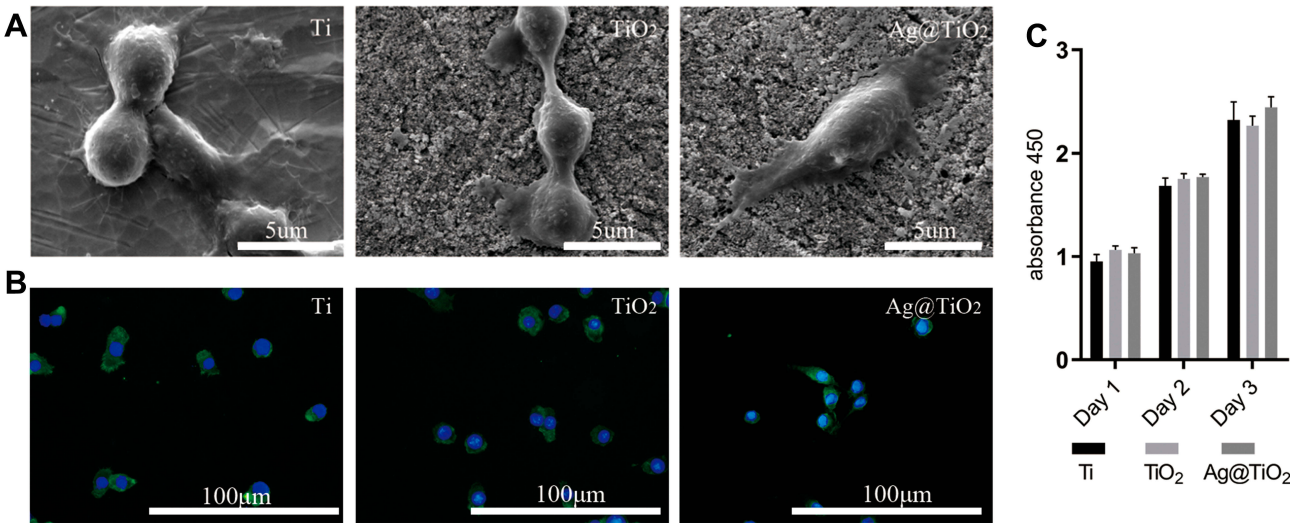

Figure 2 Cell morphology and proliferation of macrophages cultured on surface of different specimens. (**A**) SEM images and (**B**) fluorescent images of the phalloidin and DAPI staining for RAW 264.7 macrophages cultured on the surface of Ti, TiO_2-NTs and Ag@TiO_2-NTs respectively. (**C**) the CCK-8 test for the proliferation RAW264.7 macrophages on Ti, TiO_2-NTs, and Ag@TiO_2-NTs. The error bars indicate means ± standard deviations.

proliferation, we loaded ultra-low-concentration of AgNPs (about 0.2ppm released at the first 24h) on TiO_2 nanotubes as mentioned above (Figure 1F), which had no significant cytotoxicity by CCK-8 test (Figure 2C). Besides, we also used the culture medium containing different concentration of AgNPs (0, 0.05, 0.10, 0.20, 0.50 and 2.0ppm) to treat macrophages (Figure S1C). The CCK-8 test showed that there was no significant difference within all groups on day 1. However, the proliferation rate of 0.5 and 2.0ppm groups was seriously impaired at day 2 and 3, while the proliferation rates of AgNPs ≤ 0.20ppm groups had not been inhibited. In conclusion, the Ag@TiO_2-NTs with the ultra-low-dose content of AgNPs had no significant cytotoxicity.

Glucose Metabolism, Autophagy, and Macrophages Polarization on the Different Surfaces

Glucose is one of the most important energies and carbon source for cells, and transported across the plasma membrane by GLUT transporters.[53] In addition, GLUT1 plays an essential role in macrophage polarization towards pro-inflammatory M1 phenotype.[29] Hence, regulating the glucose metabolism in macrophages is an effective strategy to eliminate inflammatory response.[54] Meanwhile, it has been proven that AgNPs has the ability to suppress the expression of GLUT1 in cells.[55] Thus, we intended to explore whether Ag@TiO_2-NTs could regulate macrophages polarization by GLUT1. Macrophages were cultured for 24h on different surfaces. GLUT1, autophagy (p62, Beclin1, LC3), M1 (iNOS), and M2 (Arginase1) markers of macrophages were analyzed by Western blot, qPCR, and immunofluorescence staining. As shown in Figure 3A, C and D, the expression level of iNOS, p62 and GLUT1 analyzed by qPCR and Western blot varied significantly among the groups: Ti > TiO_2-NTs > Ag@TiO_2-NTs. In contrast, the expression level of Arginase1, Beclin1 and LC3 was opposite: Ti < TiO_2-NTs < Ag@TiO_2-NTs. These results indicated a lower GLUT1 expression, and a higher autophagy level as well as anti-inflammation status of Ag@TiO_2-NTs group. To further demonstrate that GLUT1 could influence the activity of autophagy, we used STF31 to treat macrophages on Ag@TiO_2-NTs. The iNOS, GLUT1 and p62 level declined significantly, while Arginase1, Beclin1, and LC3 level increased significantly compared with the level of Ag@TiO_2-NTs group. Moreover, the immunofluorescence staining for GLUT1 verified the trend of qPCR and Western blot on individual groups: Ti >TiO_2-NTs >Ag@TiO_2-NTs > Ag@TiO_2-NTs+STF31 (Figure 3B). Interestingly, Wei et al also reported that autophagy might be regulated by glucose metabolism,[56] which was consistent with our results. Autophagy is a ubiquitously conserved cellular process, which can regulate intracellular homeostasis and immunity[2] and alleviate the oxidative stress via eliminating ROS.[57] To explore the influence of autophagy, the markers of autophagy and polarization were analyzed by Western blot (Figure 4A and B) and qPCR (Figure 4C). Ag@TiO_2-NTs promoted the expression of LC3, Beclin1, and Arginase1, whereas inhibited the expression of p62, and iNOS comparing with pure Ti and TiO_2-NTs. However, there was no significant difference between Ti and TiO_2-NTs groups. The immunofluorescence staining also verified this trend (Figure 5A and C). Besides, we used 3-MA and rapamycin to treat macrophages cultured on Ag@TiO_2-NTs (Figure 4A and B). Comparing with untreated macrophages on Ag@TiO_2-NTs, the expression of LC3, Beclin1 and Arginase1 decreased, whereas the expression of p62 and iNOS increased after treated by 3-MA. However, in the Ag@TiO_2-NTs+3MA+Rapa group, the expression of LC3, Beclin1 and Arginase1 increased, and the p62 and iNOS declined compared with the expression of Ag@TiO_2-NTs +3MA group. These results indicated that Ag@TiO_2-NTs may stimulate autophagy and promote M2 polarization. This polarization shift has been widely reported to promote satisfied tissue repair and bone integration around the implant.[58]

To further investigate the relationship between Ag^+ ions concentration and its immunoregulatory function, we cultured macrophages with medium containing different concentrations of AgNPs (0 ~ 2.0 ppm) (Figure S1D–F). Compared with the control group, macrophages expressed more Arginase1 and fewer iNOS when the concentration of AgNPs ≤ 0.20 ppm, which indicated the trend of M2 polarization instead of M1 polarization. However, both the M1 and M2 markers declined when the concentration of AgNPs > 0.20 ppm, which may be explained by the significant toxic effects (Figure S1C). As a result, the concentration of AgNPs seems to be an important factor in regulating the immune response. And the TiO_2-NTs, as a sustained release platform, are critical to maintaining the suitable concentration in local.

Thus, Ag@TiO_2-NTs have the satisfying ability to promote M2 polarization and inhibit M1 polarization via inhibiting the expression of GLUT1, and promoting autophagy (Scheme 1).

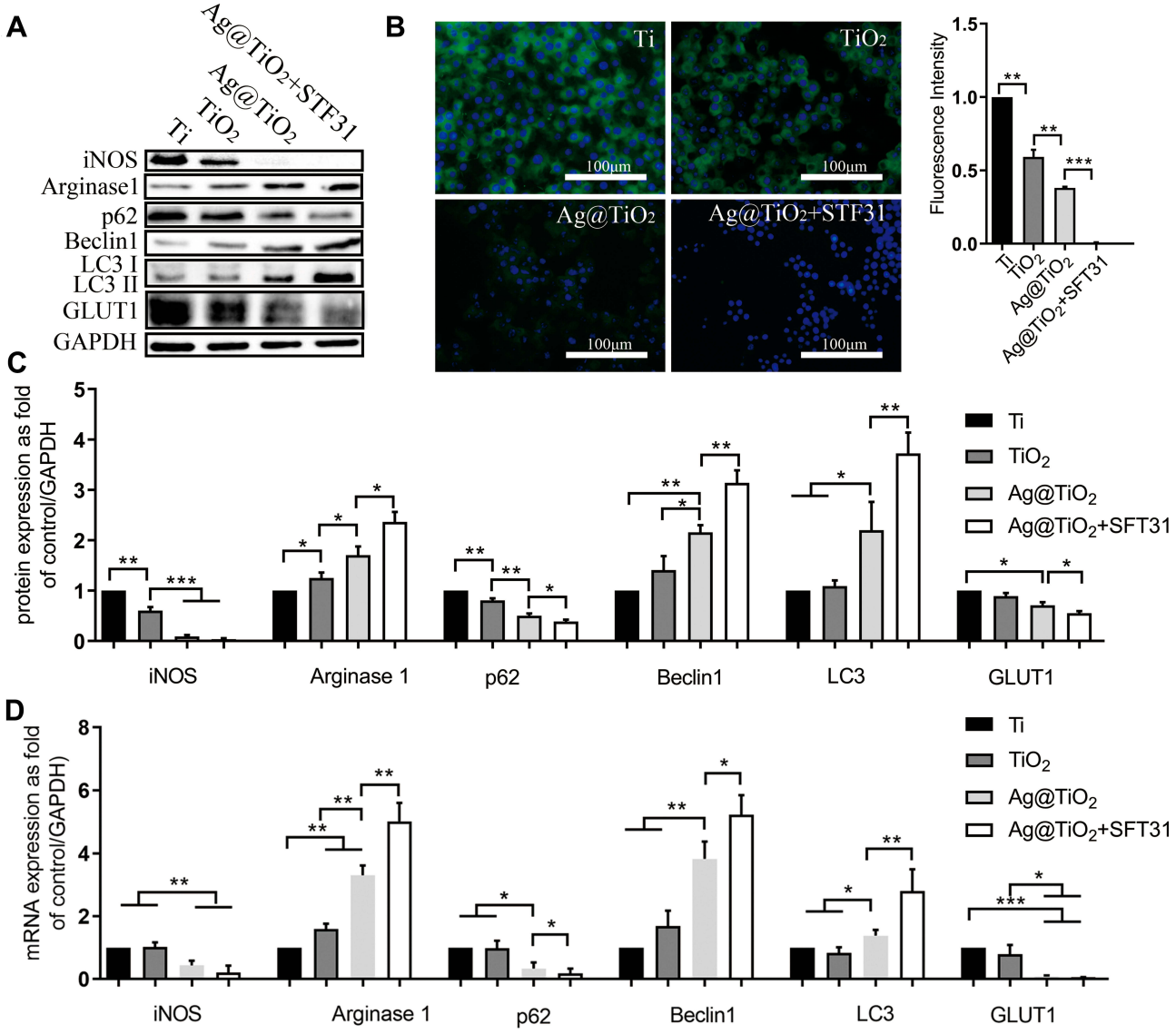

Figure 3 Glucose metabolism, autophagy, and macrophages polarization on the different surfaces. (**A, C**) Western blot analysis and (**D**) qPCR analysis of iNOS, Arginase1, p62, Beclin1, LC3, GLUT 1 and GAPDH in macrophages cultured on Ti, TiO_2-NTs, Ag@TiO_2-NTs, and Ag@TiO_2-NTs+STF31. (**B**) Immunofluorescent staining for GLUT1 in macrophages cultured on Ti, TiO_2-NTs, Ag@TiO_2-NTs, Ag@TiO_2-NTs+STF31. The error bars indicate means ± standard deviations: *p<0.05, **p<0.01 and ***p<0.001.

The Antioxidant Ability of the Different Surfaces

ROS is the byproduct of many enzymatic reactions, which plays a key role in cellular homeostasis and dysfunction.[59] The implant surgery will lead to an oxidative environment around the implant for the reason of surgical trauma.[2] For immune response, oxidative stress is the important inducer of M1 macrophage and over-production of ROS will impair the homeostasis of local tissues and cells.[59] Meanwhile, ROS can promote the migration of inflammatory cells to the local area, which is harmful to bone healing.[60] Many biomaterials contributed to tissue regeneration through ROS scavenging in multiple fields, such as skin wound,[61] bone defect,[62] and myocardial infarction.[63] The FRAP test showed there was no prominent antioxidant ability on pure Ti and TiO_2-NTs groups, but Ag@TiO_2-NTs exhibited significant ROS scavenging efficiency (Figure 5E). Besides, we used the DCFH-DA probe to test the intracellular ROS production in macrophages (Figure 5B and D). The DCFH-DA fluorescence intensity, visualized by confocal microscopy, was lower on Ag@TiO_2-NTs than the intensity on Ti and TiO_2-NTs. To explore whether autophagy induction can remove the ROS from cells, we used 3-MA and 3-MA+Rapa treatment for Ag@TiO_2-NT groups, which showed that the

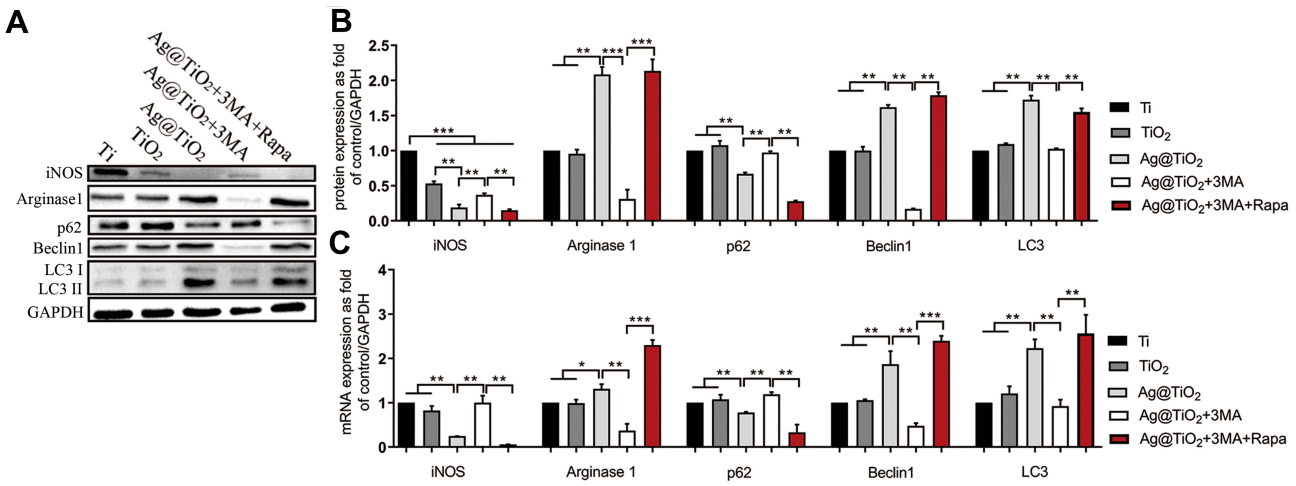

Figure 4 The influences of different surfaces on autophagy and polarization of macrophages. (**A, B**) Western blot analysis and (**C**) qPCR analysis of iNOS, Arginase1, p62, Beclin1, LC3 and GAPDH in macrophages cultured on Ti, TiO_2-NTs, Ag@TiO_2-NTs, Ag@TiO_2-NTs+3MA and Ag@TiO_2-NTs+3MA+Rapa. The error bars indicate means ± standard deviations: *p<0.05, **p<0.01 and ***p<0.001.

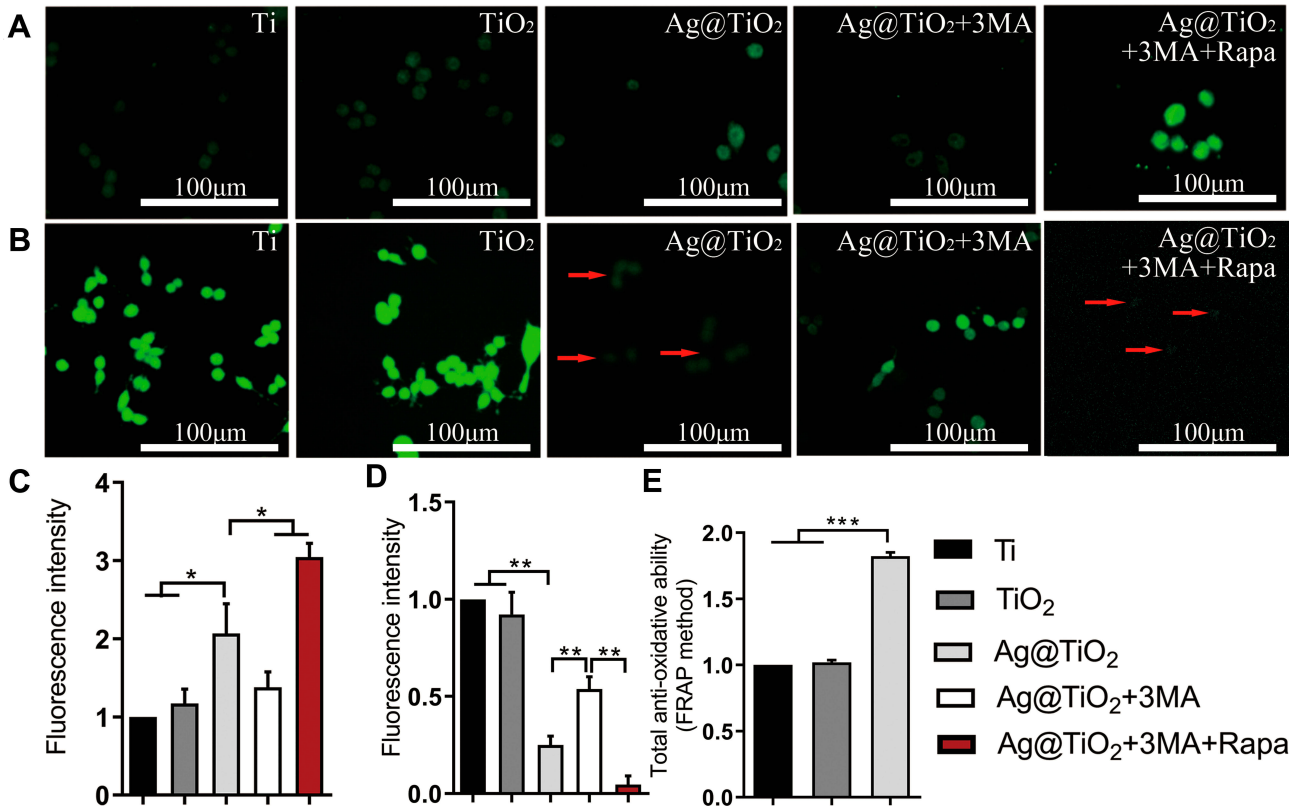

Figure 5 Fluorescence staining and analysis of LC3 and ROS. (**A, C**) LC3-Immunofluorescence staining and analysis. (**B, D**) DCFH-DA probe fluorescence analysis for RAW264.7 macrophages grown on Ti, TiO_2-NTs, Ag@TiO_2-NTs, Ag@TiO_2-NTs+3MA and Ag@TiO_2-NTs+3MA+Rapa. (**E**) the total antioxidant capacity of Ti, TiO_2-NTs and Ag@TiO_2-NTs that evaluated by the FRAP method.The error bars indicate means ± standard deviations: *p<0.05, and **p<0.01.

fluorescence intensity increased and decreased significantly in DCFH-DA fluorescence test, respectively. Moreover, the different concentrations of AgNPs test revealed that the production of ROS increased significantly if the concentration of AgNPs>0.20 ppm, while the production of ROS was significantly lower if AgNPs ≤ 0.20 ppm (Figure S1A and B). Although some researchers reported that AgNPs had an antioxidant effect,[64–68] we attributed this property to the ultra-low concentration (≤ 0.20ppm) of AgNPs. The results demonstrated that the Ag@TiO_2-NTs group exhibited

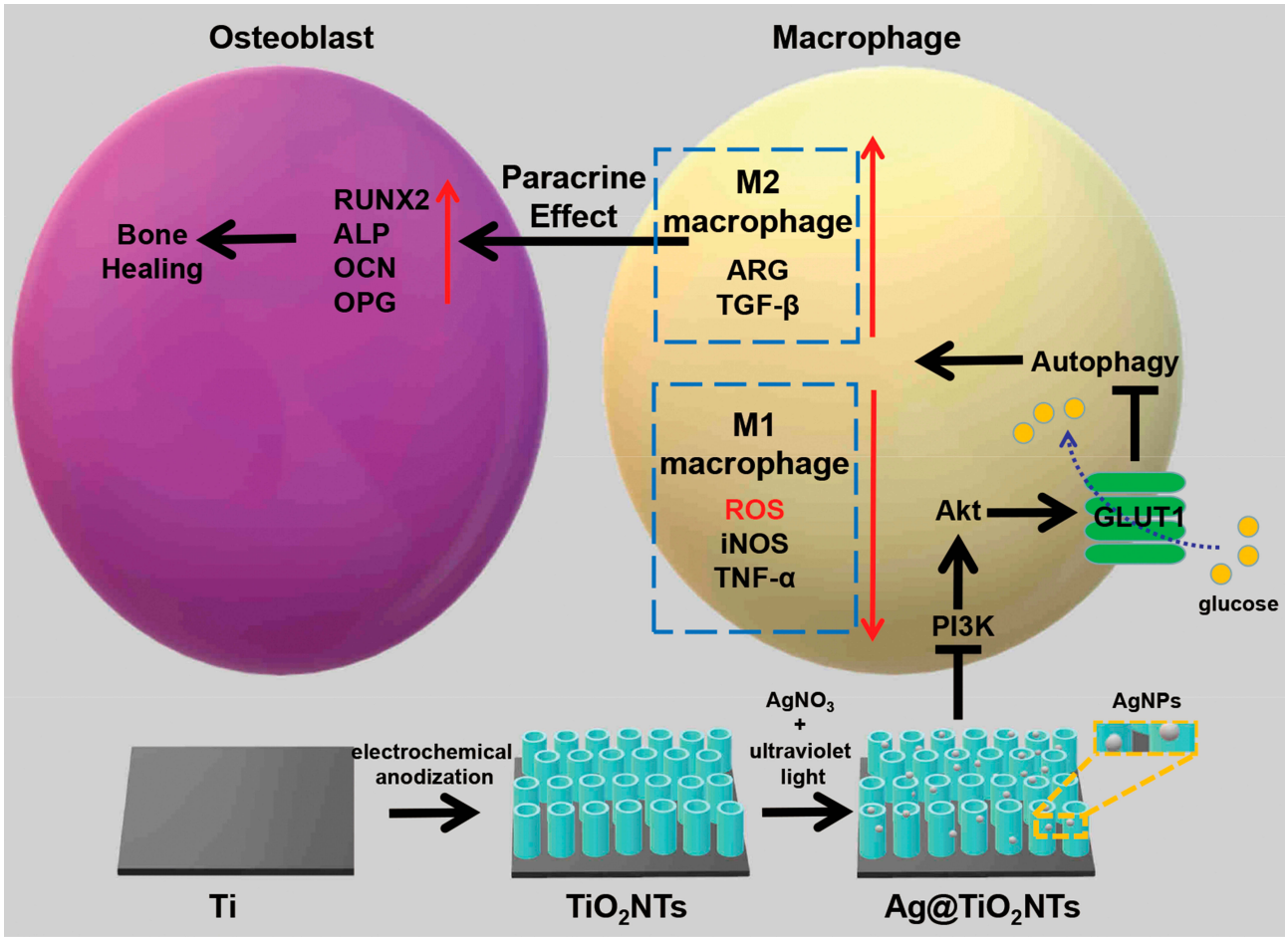

Scheme 1 The behavior of the macrophage cell and osteoblast cell modulated by Ag@TiO_2-NTs.

satisfied ROS scavenging capacity, and the antioxidant ability of AgNPs was dose-dependent.

Ag@TiO2-NTs Suppress PI3K/Akt Pathway

To further explore the molecular mechanism, we intended to study the PI3K/Akt pathway signaling pathway. It has been reported that PI3K/Akt was the upstream regulator of GLUT1 and played a key role in a wide range of cellular activities, such as the bone healing, osteoclast formation, endothelialization, and inflammation.[4,69] But the role of the PI3K/Akt pathway in the inflammation response of biomaterials is not clear. In this study, we used 740Y-P to activate the PI3K/Akt pathway of Ag@TiO2-NTs group, and the immunofluorescence staining (Figure 6A), western-blot (Figure 6B and C) and qPCR (Figure 6D) indicated that the expression of p-Akt on Ag@TiO_2-NTs was the lowest compared with the expression of Ti and TiO_2-NTs groups. In addition, the expression of p-Akt and GLUT1 increased and LC3 decreased significantly in the Ag@TiO_2-NTs+740Y-P group compared with the untreated Ag@TiO_2-NTs group. In conclusion, Ag@TiO_2-NTs could inhibit GLUT1 and promote autophagy levels in macrophages via suppressing PI3K/Akt pathway (Scheme 1).

Osteo-Immunoregulatory Ability in vitro

Focused on the interaction between bone healing and the immune response, "Osteo-immunology" characterizes the molecular mechanism between the immune response and bone healing.[4,69] The necessary regulation of the immune cells and cytokines is indispensable for the bone healing process, but inappropriate recruiting and activating of the immune cells will lead to bone metabolism derangement.[70] Thus, we used the traditional co-culture method to treat MC3T3-E1 pre-osteoblasts with macrophage CM to study the osteo-immunomodulatory ability of Ag@TiO_2-NTs. The results showed that the CM of Ag@TiO_2-NTs group significantly promoted the osteogenic gene expression of ALP

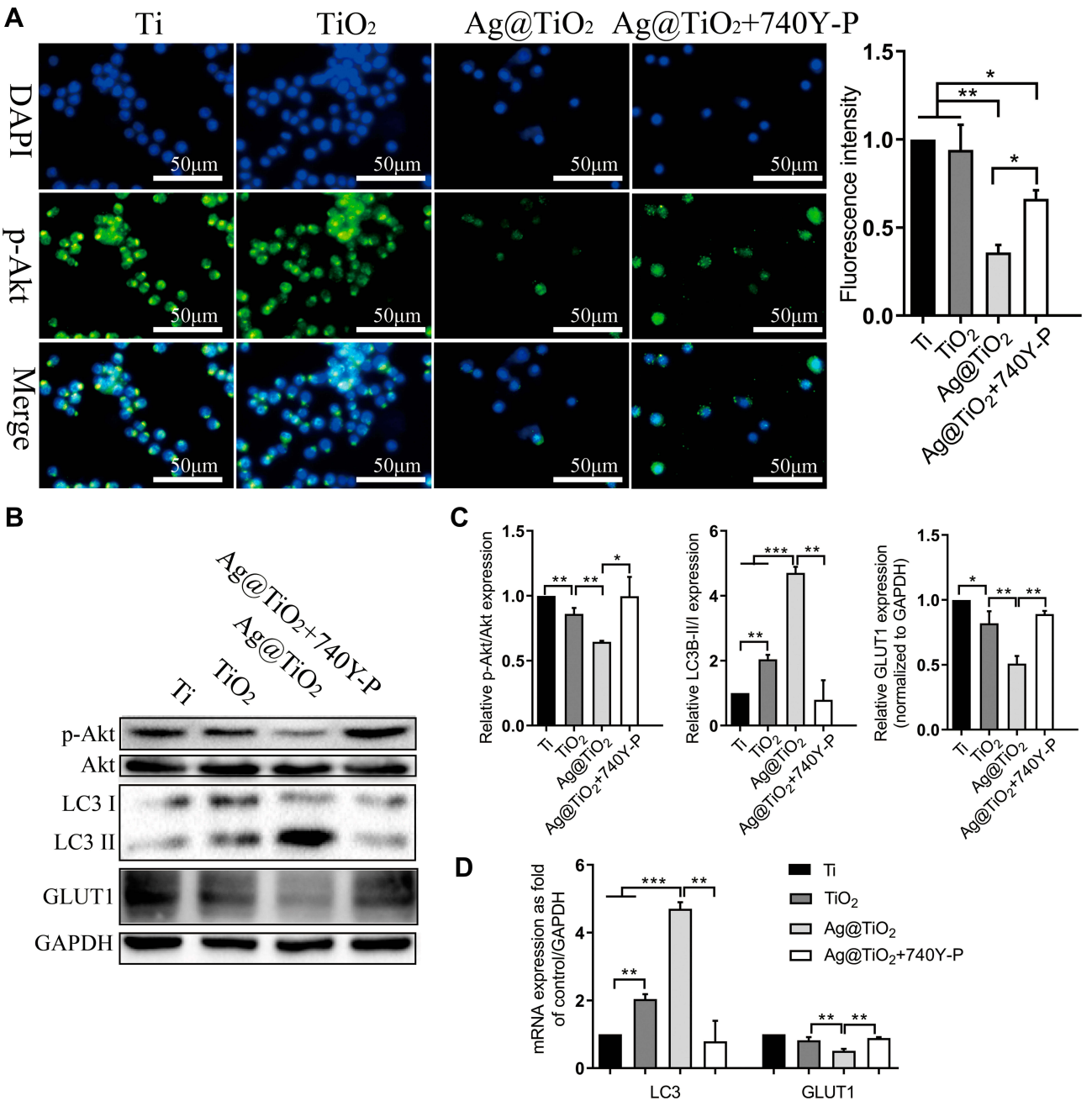

Figure 6 The influences of different surfaces on PI3K/Akt pathway. (**A**) p-Akt immunofluorescence staining and analysis. (**B, C**) Western blot analysis of p-Akt, Akt, LC3, GLUT 1 and GAPDH, and (**D**) gene expression analysis of LC3 and GLUT 1 for RAW264.7 macrophages cultured on Ti, TiO_2-NTs, Ag@TiO_2-NTs, and Ag@TiO_2-NTs +740Y-P. The error bars indicate means ± standard deviations: *p<0.05, **p<0.01 and ***p<0.001.

(Figure 7A) and RUNX2 in osteoblasts (Figure 7B). Besides, we conducted the alizarin red staining (Figure 7C) and ALP staining (Figure 7D) after 21 and 7 days. The results showed that the Ag@TiO_2-NTs CM group had a significantly stronger osteogenic tendency, compared with the Ti and TiO_2-NT CM groups. These results revealed that Ag@TiO_2-NTs had the satisfying ability to create an osteo-immune microenvironment in vitro.

Osteo-Immunoregulatory Ability in vivo

Finally, we performed an animal experiment by using a tibial defect model with the biomaterials implanted in the marrow cavity. 2 weeks after surgery, the bone healing status was evaluated by X-ray evaluation, micro-CT, and immunohistochemical staining. The X-ray images (Figure 7E) showed that the defect of the tibia (red arrow) was still obvious around the Ti implant and TiO_2-NTs implant. However, the

new tibial cortex without obvious defect was detected around the Ag@TiO_2-NTs implant. The transverse 3D images (Figure 7B and F) were used to provide specific information on the implant osteointegration and peri-implant trabecular microstructure by Qualitative micro-CT. Compared with Ti and TiO_2-NTs implants, more trabeculae was observed around the Ag@TiO_2-NTs. In addition, the Ag@TiO_2-NTs groups exhibited a higher BV/TV ratio significantly, which indicated the satisfied osteogenic competence.

Furthermore, the immunohistochemical staining showed a higher expression level of TGF-β (Figure 7G) and LC3 (Figure 7I) around the Ag@TiO_2-NTs implants, indicated a larger number of M2 macrophages and higher autophagy level were arisen at local. Meanwhile, a lower expression level of TNF-α (Figure 7H), p-Akt (Figure 7J), GLUT1 (Figure 7K) were detected around the Ag@TiO_2-NTs implant, demonstrated that the M1 polarization, p-Akt, and its downstream effector GLUT1 were inhibited.

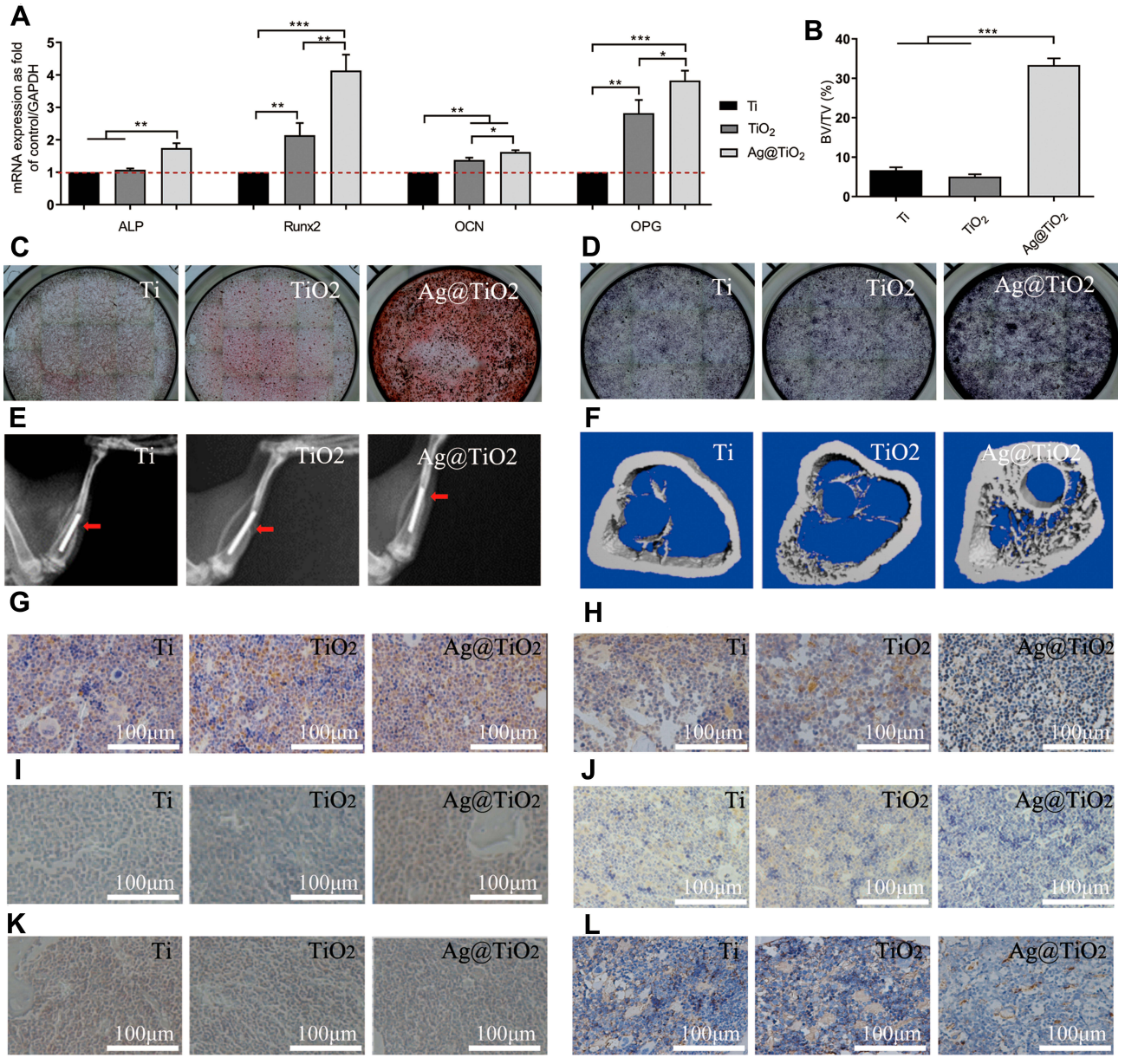

Figure 7 Osteogenic ability in vitro and in vivo. MC3T3-E1 gene expression for (**A**) ALP, RUNX2, OCN and OPG. (**C**) alizarin red staining and (**D**) ALP for MC3T3-E1 cells. (**E**) The healing status of bone defect was evaluated by X-ray 2 weeks after surgery. (**F**) Micro-CTwere used to evaluate new bone formation and (**B**) the bone volume/tissue volume (BV/TV) ratio. Immunohistochemical staining for (**G**) TGF-β, (**H**) TNF-α, (**I**) LC3, (**J**) p-Akt, (**K**) GLUT1and (**L**) CD68, the surface of Ag@TiO_2-NTs significantly promoted the expression of TGF-β, LC3, whereas inhibited the expression of TNF-α, p-Akt, GLUT1and CD68. The error bars indicate means ± standard deviations: *p<0.05, **p<0.01, ***p<0.001.

More importantly, the decline of CD68 (Figure 7L) indicated a reduction in the number of macrophages around Ag@TiO_2-NTs implant. The micro-environment containing the decreased number of $CD68^+$ macrophages with the lower rate of M1/M2 has been reported to be dispensable for an excellent osteo-immune microenvironment and promote osteogenesis. As a result, our study revealed that Ag@TiO_2-NTs had the satisfying ability to facilitate M2 macrophage polarization, create an osteo-immune microenvironment, and promote bone healing by suppressing p-Akt, GLUT1, and activating autophagy in vivo.

Conclusion

Our present study had fabricated a surface modification of Ag@TiO_2-NTs with ultra-low-dose AgNPs, which could facilitate the polarization of macrophages towards the M2 phenotype, inhibit inflammation, and promote bone formation by inhibiting PI3K/Akt and GLUT1, activating autophagy, and scavenging ROS in vitro. Besides, the satisfied bone formation was detected with the osteo-immune microenvironment created by the increasing number of wound healing the M2 macrophage around Ag@TiO_2-NTs in vivo. As an antibacterial material, Ag@TiO_2-NTs with ultra-low-dose AgNPs exhibited simultaneous immuno-regulatory ability and excellent osteogenic capability, made it a promising biomaterial for implants application.

Acknowledgments

This work was supported by funding from the National Natural Science Foundation of China (NO. 81571816; NO.81601611). Yangmengfan Chen and Ming Guan are also supported by the fellowship from the China Scholarship Council.

Disclosure

The authors have declared that no competing interest exists and that they have no conflicts of interest in this work.

References

1. Meyerink JG, Kota D, Wood ST, Crawford GA. Transparent titanium dioxide nanotubes: processing, characterization, and application in establishing cellular response mechanisms. *Acta Biomater*. 2018;79:364–374. doi:10.1016/j.actbio.2018.08.039
2. Keegan GM, Learmonth ID, Case CP. A systematic comparison of the actual, potential, and theoretical health effects of cobalt and chromium exposures from industry and surgical implants. *Crit Rev Toxicol*. 2008;38(8):645–674. doi:10.1080/10408440701845534
3. Wang N, Li H, Lu W, et al. Effects of TiO2 nanotubes with different diameters on gene expression and osseointegration of implants in minipigs. *Biomaterials*. 2011;32(29):6900–6911. doi:10.1016/j.biomaterials.2011.06.023
4. Xu WC, Dong X, Ding JL, et al. Nanotubular TiO2 regulates macrophage M2 polarization and increases macrophage secretion of VEGF to accelerate endothelialization via the ERK1/2 and PI3K/AKT pathways. *Int J Nanomedicine*. 2019;14:441–455. doi:10.2147/IJN.S188439
5. Bhardwaj G, Webster TJ. Reduced bacterial growth and increased osteoblast proliferation on titanium with a nanophase TiO2 surface treatment. *Int J Nanomed*. 2017;12:363–369. doi:10.2147/IJN.S116105
6. Gao A, Hang R, Huang X, et al. The effects of titania nanotubes with embedded silver oxide nanoparticles on bacteria and osteoblasts. *Biomaterials*. 2014;35(13):4223–4235. doi:10.1016/j.biomaterials.2014.01.058
7. Guan M, Chen Y, Wei Y, et al. Long-lasting bactericidal activity through selective physical puncture and controlled ions release of polydopamine and silver nanoparticles-loaded TiO2 nanorods in vitro and in vivo. *Int J Nanomed*. 2019;14:2903–2914. doi:10.2147/IJN.S202625
8. Cheng H, Xiong W, Fang Z, et al. Strontium (Sr) and silver (Ag) loaded nanotubular structures with combined osteoinductive and antimicrobial activities. *Acta Biomater*. 2016;31:388–400. doi:10.1016/j.actbio.2015.11.046
9. Cheng H, Li Y, Huo K, Gao B, Xiong W. Long-lasting in vivo and in vitro antibacterial ability of nanostructured titania coating incorporated with silver nanoparticles. *J Biomed Mater Res A*. 2014;102(10):3488–3499. doi:10.1002/jbm.a.35019
10. Xu N, Cheng H, Xu J, et al. Silver-loaded nanotubular structures enhanced bactericidal efficiency of antibiotics with synergistic effect in vitro and in vivo. *Int J Nanomedicine*. 2017;12:731–743. doi:10.2147/IJN.S123648
11. Gao C, Cheng H, Xu N, et al. Poly(dopamine) and Ag nanoparticle-loaded TiO2 nanotubes with optimized antibacterial and ROS-scavenging bioactivities. *Nanomedicine (Lond)*. 2019;14(7):803–818. doi:10.2217/nnm-2018-0131
12. Zeng X, Xiong S, Zhuo S, et al. Nanosilver/poly (dl-lactic-co-glycolic acid) on titanium implant surfaces for the enhancement of antibacterial properties and osteoinductivity. *Int J Nanomedicine*. 2019;14:1849–1863. doi:10.2147/IJN.S190954
13. Xue Y, Hong X, Gao J, Shen R, Ye Z. Preparation and biological characterization of the mixture of poly(lactic-co-glycolic acid)/chitosan/Ag nanoparticles for periodontal tissue engineering. *Int J Nanomedicine*. 2019;14:483–498. doi:10.2147/IJN.S184396
14. Saleh LS, Bryant SJ. The host response in tissue engineering: crosstalk between immune cells and cell-laden scaffolds. *Curr Opin Biomed Eng*. 2018;6:58–65. doi:10.1016/j.cobme.2018.03.006
15. Schlundt C, Schell H, Goodman SB, Vunjak-Novakovic G, Duda GN, Schmidt-Bleek K. Immune modulation as a therapeutic strategy in bone regeneration. *J Exp Orthop*. 2015;2(1):1. doi:10.1186/s40634-014-0017-6
16. Ma QL, Zhao LZ, Liu RR, et al. Improved implant osseointegration of a nanostructured titanium surface via mediation of macrophage polarization. *Biomaterials*. 2014;35(37):9853–9867. doi:10.1016/j.biomaterials.2014.08.025
17. Mills CD, Kincaid K, Alt JM, Heilman MJ, Hill AM. M-1/M-2 macrophages and the Th1/Th2 paradigm. *J Immunol*. 2000;164(12):6166–6173. doi:10.4049/jimmunol.164.12.6166
18. Yang D, Wan Y. Molecular determinants for the polarization of macrophage and osteoclast. *Semin Immunopathol*. 2019;41(5):551–563. doi:10.1007/s00281-019-00754-3
19. Tardito S, Martinelli G, Soldano S, et al. Macrophage M1/M2 polarization and rheumatoid arthritis: a systematic review. *Autoimmun Rev*. 2019;18(11):102397. doi:10.1016/j.autrev.2019.102397
20. Ruytinx P, Proost P, Van Damme J, Struyf S. Chemokine-induced macrophage polarization in inflammatory conditions. *Front Immunol*. 2018;9:1930. doi:10.3389/fimmu.2018.01930
21. Orecchioni M, Ghosheh Y, Pramod AB, Ley K. Macrophage polarization: different gene signatures in M1(LPS+) vs. classically and M2 (LPS-) vs. alternatively activated macrophages. *Front Immunol*. 2019;10:1084. doi:10.3389/fimmu.2019.01084

22. Lee CH, Kim YJ, Jang JH, Park JW. Modulating macrophage polarization with divalent cations in nanostructured titanium implant surfaces. *Nanotechnology*. 2016;27(8):085101. doi:10.1088/0957-4484/27/8/085101
23. Rao AJ, Gibon E, Ma T, Yao Z, Smith RL, Goodman SB. Revision joint replacement, wear particles, and macrophage polarization. *Acta Biomater*. 2012;8(7):2815–2823. doi:10.1016/j.actbio.2012.03.042
24. Guihard P, Danger Y, Brounais B, et al. Induction of osteogenesis in mesenchymal stem cells by activated monocytes/macrophages depends on oncostatin M signaling. *Stem Cells*. 2012;30(4):762–772. doi:10.1002/stem.1040
25. Park JH, Cho HJ, Kim DD. Poly((D,L)lactic-glycolic)acid-star glucose nanoparticles for glucose transporter and hypoglycemia-mediated tumor targeting. *Int J Nanomed*. 2017;12:7453–7467. doi:10.2147/IJN.S147668
26. Coronel MM, Geusz R, Stabler CL. Mitigating hypoxic stress on pancreatic islets via in situ oxygen generating biomaterial. *Biomaterials*. 2017;129:139–151. doi:10.1016/j.biomaterials.2017.03.018
27. Koo SJ, Garg NJ. Metabolic programming of macrophage functions and pathogens control. *Redox Biol*. 2019;24:101198. doi:10.1016/j.redox.2019.101198
28. Ali L, Schnitzler JG, Kroon J. Metabolism: the road to inflammation and atherosclerosis. *Curr Opin Lipidol*. 2018;29(6):474–480. doi:10.1097/MOL.0000000000000550
29. Freemerman AJ, Johnson AR, Sacks GN, et al. Metabolic reprogramming of macrophages: glucose transporter 1 (GLUT1)-mediated glucose metabolism drives a proinflammatory phenotype. *J Biol Chem*. 2014;289(11):7884–7896. doi:10.1074/jbc.M113.522037
30. Clarke AJ, Simon AK. Autophagy in the renewal, differentiation and homeostasis of immune cells. *Nat Rev Immunol*. 2019;19(3):170–183. doi:10.1038/s41577-018-0095-2
31. Lahiri V, Hawkins WD, Klionsky DJ. Watch what you (Self-) eat: autophagic mechanisms that modulate metabolism. *Cell Metab*. 2019;29(4):803–826. doi:10.1016/j.cmet.2019.03.003
32. Deretic V, Saitoh T, Akira S. Autophagy in infection, inflammation and immunity. *Nat Rev Immunol*. 2013;13(10):722–737. doi:10.1038/nri3532
33. Zhou R, Yazdi AS, Menu P, Tschopp J. A role for mitochondria in NLRP3 inflammasome activation. *Nature*. 2011;469(7329):221–225. doi:10.1038/nature09663
34. Saitoh T, Fujita N, Jang MH, et al. Loss of the autophagy protein Atg16L1 enhances endotoxin-induced IL-1beta production. *Nature*. 2008;456(7219):264–268. doi:10.1038/nature07383
35. Nakahira K, Haspel JA, Rathinam VAK, et al. Autophagy proteins regulate innate immune responses by inhibiting the release of mitochondrial DNA mediated by the NALP3 inflammasome. *Nat Immunol*. 2011;12(3):222–230. doi:10.1038/ni.1980
36. Liu K, Zhao E, Ilyas G, et al. Impaired macrophage autophagy increases the immune response in obese mice by promoting proinflammatory macrophage polarization. *Autophagy*. 2015;11(2):271–284. doi:10.1080/15548627.2015.1009787
37. Dupont N, Jiang S, Pilli M, Ornatowski W, Bhattacharya D, Deretic V. Autophagy-based unconventional secretory pathway for extracellular delivery of IL-1beta. *EMBO J*. 2011;30(23):4701–4711. doi:10.1038/emboj.2011.398
38. Song M, Han L, Chen FF, et al. Adipocyte-derived exosomes carrying sonic hedgehog mediate M1 macrophage polarization-induced insulin resistance via Ptch and PI3K pathways. *Cell Physiol Biochem*. 2018;48(4):1416–1432. doi:10.1159/000492252
39. Atif F, Yousuf S, Espinosa-Garcia C, Sergeeva E, Stein DG. Progesterone treatment attenuates glycolytic metabolism and induces senescence in glioblastoma. *Sci Rep*. 2019;9(1):988. doi:10.1038/s41598-018-37399-5
40. Kim YC, Guan KL. mTOR: a pharmacologic target for autophagy regulation. *J Clin Invest*. 2015;125(1):25–32. doi:10.1172/JCI73939
41. Lv L, Xie Y, Li K, et al. Unveiling the mechanism of surface hydrophilicity-modulated macrophage polarization. *Adv Healthc Mater*. 2018;7(19):e1800675. doi:10.1002/adhm.201800675
42. Sun SJ, Yu WQ, Zhang YL, Jiang XQ, Zhang FQ. Effects of TiO2 nanotube layers on RAW 264.7 macrophage behaviour and bone morphogenetic protein-2 expression. *Cell Prolif*. 2013;46(6):685–694. doi:10.1111/cpr.12072
43. Rajyalakshmi A, Ercan B, Balasubramanian K, Webster TJ. Reduced adhesion of macrophages on anodized titanium with select nanotube surface features. *Int J Nanomedicine*. 2011;6:1765–1771. doi:10.2147/IJN.S22763
44. Liu W, Golshan NH, Deng X, et al. Selenium nanoparticles incorporated into titania nanotubes inhibit bacterial growth and macrophage proliferation. *Nanoscale*. 2016;8(34):15783–15794. doi:10.1039/c6nr04461a
45. Zong M, Bai L, Liu Y, et al. Antibacterial ability and angiogenic activity of Cu-Ti-O nanotube arrays. *Mater Sci Eng C Mater Biol Appl*. 2017;71:93–99. doi:10.1016/j.msec.2016.09.077
46. Venugopal A, Muthuchamy N, Tejani H, et al. Incorporation of silver nanoparticles on the surface of orthodontic microimplants to achieve antimicrobial properties. *Korean J Orthod*. 2017;47(1):3–10. doi:10.4041/kjod.2017.47.1.3
47. Zhao L, Wang H, Huo K, et al. Antibacterial nano-structured titania coating incorporated with silver nanoparticles. *Biomaterials*. 2011;32(24):5706–5716. doi:10.1016/j.biomaterials.2011.04.040
48. Gongadze E, Kabaso D, Bauer S, Park J, Schmuki P, Iglic A. Adhesion of osteoblasts to a vertically aligned TiO2 nanotube surface. *Mini Rev Med Chem*. 2013;13(2):194–200.
49. Andree L, Barata D, Sutthavas P, Habibovic P, van Rijt S. Guiding mesenchymal stem cell differentiation using mesoporous silica nanoparticle-based films. *Acta Biomater*. 2019;96:557–567. doi:10.1016/j.actbio.2019.07.008
50. Shim JS, Kim HC, Park SI, Yun HJ, Ryu JJ. Comparison of various implant provisional resin materials for cytotoxicity and attachment to human gingival fibroblasts. *Int J Oral Maxillofac Implants*. 2019;34(2):390–396. doi:10.11607/jomi.6707
51. Pauksch L, Hartmann S, Rohnke M, et al. Biocompatibility of silver nanoparticles and silver ions in primary human mesenchymal stem cells and osteoblasts. *Acta Biomater*. 2014;10(1):439–449. doi:10.1016/j.actbio.2013.09.037
52. Qian Y, Zhou X, Zhang F, Diekwisch TGH, Luan X, Triple YJ. PLGA/PCL scaffold modification including silver impregnation, collagen coating, and electrospinning significantly improve biocompatibility, antimicrobial, and osteogenic properties for orofacial tissue regeneration. *ACS Appl Mater Interfaces*. 2019;11(41):37381–37396. doi:10.1021/acsami.9b07053
53. Lee WC, Guntur AR, Long F, Rosen CJ. Energy metabolism of the osteoblast: implications for osteoporosis. *Endocr Rev*. 2017;38(3):255–266. doi:10.1210/er.2017-00064
54. Xu C, Wang W, Zhong J, et al. Canagliflozin exerts anti-inflammatory effects by inhibiting intracellular glucose metabolism and promoting autophagy in immune cells. *Biochem Pharmacol*. 2018;152:45–59. doi:10.1016/j.bcp.2018.03.013
55. Yang T, Yao Q, Cao F, Liu Q, Liu B, Wang XH. Silver nanoparticles inhibit the function of hypoxia-inducible factor-1 and target genes: insight into the cytotoxicity and antiangiogenesis. *Int J Nanomedicine*. 2016;11:6679–6692. doi:10.2147/IJN.S109695
56. Wei R, Mao L, Xu P, et al. Suppressing glucose metabolism with epigallocatechin-3-gallate (EGCG) reduces breast cancer cell growth in preclinical models. *Food Funct*. 2018;9(11):5682–5696. doi:10.1039/c8fo01397g
57. Chen Z, Ni S, Han S, et al. Nanoporous microstructures mediate osteogenesis by modulating the osteo-immune response of macrophages. *Nanoscale*. 2017;9(2):706–718. doi:10.1039/c6nr06421c

58. Brown BN, Haschak MJ, Lopresti ST, Stahl EC. Effects of age-related shifts in cellular function and local microenvironment upon the innate immune response to implants. *Semin Immunol*. 2017;29:24–32. doi:10.1016/j.smim.2017.05.001
59. Forrester SJ, Kikuchi DS, Hernandes MS, Xu Q, Griendling KK. Reactive oxygen species in metabolic and inflammatory signaling. *Circ Res*. 2018;122(6):877–902. doi:10.1161/CIRCRESAHA.117.311401
60. Tan HY, Wang N, Li S, Hong M, Wang X, Feng Y. The reactive oxygen species in macrophage polarization: reflecting its dual role in progression and treatment of human diseases. *Oxid Med Cell Longev*. 2016;2016:2795090. doi:10.1155/2016/2795090
61. Tang P, Han L, Li P, et al. Mussel-inspired electroactive and antioxidative scaffolds with incorporation of polydopamine-reduced graphene oxide for enhancing skin wound healing. *ACS Appl Mater Interfaces*. 2019;11(8):7703–7714. doi:10.1021/acsami.8b18931
62. Li M, Chen X, Yan J, et al. Inhibition of osteoclastogenesis by stem cell-derived extracellular matrix through modulation of intracellular reactive oxygen species. *Acta Biomater*. 2018;71:118–131. doi:10.1016/j.actbio.2018.03.003
63. Shiekh PA, Singh A, Kumar A. Engineering bioinspired antioxidant materials promoting cardiomyocyte functionality and maturation for tissue engineering application. *ACS Appl Mater Interfaces*. 2018;10(4):3260–3273. doi:10.1021/acsami.7b14777
64. Park HS, Kim KH, Jang S, et al. Attenuation of allergic airway inflammation and hyperresponsiveness in a murine model of asthma by silver nanoparticles. *Int J Nanomedicine*. 2010;5:505–515. doi:10.2147/ijn.s11664
65. Manshian BB, Pfeiffer C, Pelaz B, et al. High-content imaging and gene expression approaches to unravel the effect of surface functionality on cellular interactions of silver nanoparticles. *ACS Nano*. 2015;9(10):10431–10444. doi:10.1021/acsnano.5b04661
66. Liu Y, Yu H, Zhang X, et al. The protective role of autophagy in nephrotoxicity induced by bismuth nanoparticles through AMPK/mTOR pathway. *Nanotoxicology*. 2018;12(6):586–601. doi:10.1080/17435390.2018.1466932
67. Li JJ, Hartono D, Ong CN, Bay BH, Yung LY. Autophagy and oxidative stress associated with gold nanoparticles. *Biomaterials*. 2010;31(23):5996–6003. doi:10.1016/j.biomaterials.2010.04.014
68. Alessandrini F, Vennemann A, Gschwendtner S, et al. Pro-inflammatory versus immunomodulatory effects of silver nanoparticles in the lung: the critical role of dose, size and surface modification. *Nanomaterials (Basel)*. 2017;7(10):300. doi:10.3390/nano7100300
69. Pan JM, Wu LG, Cai JW, Wu LT, Liang M. Dexamethasone suppresses osteogenesis of osteoblast via the PI3K/Akt signaling pathway in vitro and in vivo. *J Recept Signal Transduct Res*. 2019;39(1):80–86. doi:10.1080/10799893.2019.1625061
70. Chen Z, Bachhuka A, Wei F, et al. Nanotopography-based strategy for the precise manipulation of osteoimmunomodulation in bone regeneration. *Nanoscale*. 2017;9(46):18129–18152. doi:10.1039/c7nr05913b